Biochimie 182 (2021) 61–72

Contents lists available at ScienceDirect

Biochimie

journal homepage: www.elsevier.com/locate/biochi

The effect of electrospun scaffolds on the glycosaminoglycan profile of differentiating neural stem cells

Fábio F.F. Garrudo [a, b, c], Paiyz E. Mikael [a], Ke Xia [a], João C. Silva [a, b], Yilan Ouyang [a], Caitlyn A. Chapman [a], Pauline R. Hoffman [a], Yanlei Yu [a], Xiaurui Han [a], Carlos A.V. Rodrigues [b], Joaquim M.S. Cabral [b], Jorge Morgado [c], Frederico C. Ferreira [b], Robert J. Linhardt [a, *]

[a] Center for Biotechnology & Interdisciplinary Studies, Department of Chemistry & Chemical Biology, Rensselaer Polytechnic Institute, Biotechnology Center 4005, Troy, NY, 12180, USA
[b] Department of Bioengineering and iBB – Institute for Bioengineering and Biosciences, Instituto Superior Técnico, Universidade de Lisboa, Av. Rovisco Pais, 1049-001, Lisboa, Portugal
[c] Department of Bioengineering and Instituto de Telecomunicações, Instituto Superior Técnico, Universidade de Lisboa, 1049-001, Lisboa, Portugal

ARTICLE INFO

Article history:
Received 15 September 2020
Received in revised form
3 January 2021
Accepted 3 January 2021
Available online 7 January 2021

Keywords:
Neural tissue engineering
Polycaprolactone
Artificial extracellular matrix
Neural differentiation
LC-MS/MS
Hyaluronic acid

ABSTRACT

The use of electrospun scaffolds for neural tissue engineering applications allows a closer mimicry of the native tissue extracellular matrix (ECM), important for the transplantation of cells *in vivo*. Moreover, the role of the electrospun fiber mat topography on neural stem cell (NSC) differentiation remains to be completely understood. In this work REN-VM cells (NSC model) were differentiated on polycaprolactone (PCL) nanofibers, obtained by wet/wet electrospinning, and on flat glass lamellas. The obtained differentiation profile of NSCs was evaluated using immunofluorescence and qPCR analysis. Glycosaminoglycan (GAG) analysis was successfully emplyed to evaluate changes in the GAG profile of differentiating cells through the use of the highly sensitive liquid chromatography-tandem mass/mass spectrometry (LC-MS/MS) method. Our results show that both culture platforms allow the differentiation of REN-VM cells into neural cells (neurons and astrocytes) similarly. Moreover, LC-MS/MS analysis shows changes in the production of GAGs present both in cell cultures and conditioned media samples. In the media, hyaluronic acid (HA) was detected and correlated with cellular activity and the production of a more plastic extracellular matrix. The cell samples evidence changes in chondroitin sulfate (CS4S, CS6S, CS4S6S) and heparan sulfate (HS6S, HS0S), similar to those previously described *in vivo* studies and possibly associated with the creation of complex structures, such as perineural networks. The GAG profile of differentiating REN-VM cells on electrospun scaffolds was analyzed for the first time. Our results highlight the advantage of using platforms obtain more reliable and robust neural tissue-engineered transplants.

1. Introduction

Tissue engineering strategies hold great promise in the treatment of neurological diseases, the 2016 world leading cause of disability-adjusted life years (276 million) and second leading cause of death (9 million) [1]. These diseases include, but are not restricted to neurodegenerative diseases (e.g., Alzheimer's disease, Parkinson's disease, Amyloid Lateral Sclerosis), psychiatric diseases (schizophrenia, psychosis), traumatic brain injury, infectious diseases (meningitis and encephalitis), cancer (e.g., glioblastoma) and idiopathic epilepsy. Although these diseases have different etiologies they all involve the irreversible change in the central nervous system (CNS) tissue homeostasis. These diseases have enormous functional consequences for the well-being of the patients as well as family members and society in general [2]. Additionally, their incidence and prevalence have increased with life expectancy. Reversing their progress and reoccurrence in the brain tissue has not yet been achieved, but the use of neural stem cells (NSCs) represents a promising approach towards such end [3].

* Corresponding author.
E-mail address: linhar@rpi.edu (R.J. Linhardt).

https://doi.org/10.1016/j.biochi.2021.01.001
0300-9084/

Using scaffolds to support NSCs growth and differentiation is the most studied strategy in neural tissue engineering applications. Not only these scaffolds provide a physical surface for cells to attach and grow but also their surface, mechanical and topography/three-dimensional structure can be modified to guide cell migration into the tissue, promote cell differentiation and ultimately lead to its integration with the original tissue [4–7]. Further functionalization to enhance the differentiation process is also possible.

Different scaffold preparation techniques are described in the literature. Electrospinning, one of the most versatile ones, relies on the application of an electrical potential to fabricate polymeric fibers. The fibers obtained have very small diameters (micrometer to nanometer range) and have high surface areas, allowing them to mimic the extracellular matrix structure and improving cell attachment, growth and differentiation [8,9].

While electrospinning allows the production of synthetic extracellular matrix (ECM) substitutes, cells produce their own natural ECM both *in vivo* and *in vitro*. Some of the basic components of ECM include structural proteins (collagen, elastin, laminin), glycoproteins (fibronectin and vitronectin) and glycosaminoglycans (GAGs) [10]. GAGs are linear polysaccharides chains composed of repeating disaccharide subunits, that are in turn composed by dimers of D-glucuronic acid (D-GlcA) or L-iduronic acid (L-IdoA) and *N*-acetylglucosamine (GlcNAc) or *N*-acetylgalactosamine (GalNAc) bound by glycosidic bonds (α- or β- and 1,3 or 1,4). The most common disaccharide subunits include heparan sulfate (HS) (GlcAβ1-4GlcNAcα1-4), chondroitin sulfate (CS) (GlcAβ1-3GalNAcβ1-4) and hyaluronan/hyaluronic acid (HA) (GlcAβ1-3GlcNAcβ1-4). Each of the GAGs subunits (except for HA) can be enzymatically sulfated in different positions. At the cellular level this is important for the creation of structural elements for protein recognition and in the regulation of downstream biochemical intracellular cascades [11,12].

GAGs play pivoteal roles on tissue homeostasis. In the central nervous system (CNS), GAGs are an important component of the ECM and also have important functions during brain development. In their work, Singh and Bachhawat show that the most abundant GAGs in the human brain are HA, CS (chondroitin-4-sulfate and chondroitin-6-sulfate), dermatan sulfate and HS and that their content changes with the age of the donor [13]. GAGs have a critical role in maintaining neuron structure and function [14]. GAGs are also present in membrane receptors and can easily bind to proteins such as fibroblast growth factor (FGF) [15]. Not only do GAGs provide structural support to neural cells but also their profile changes according with different factors such as age and health [16,17]. In the case of Alzheimer's disease HS enriched proteoglycans of astrocytic origin co-deposite with amyloid plaques. Interestingly, sulfated GAGs are also found to promote amyloid beta (Aβ) aggregation. HS binds to tau protein, promoting different HS enriched proteoglycans that interfere with β-secretase (BACE1) cleavage of amyloid precursor protein (APP) into Aβ, the main component of amyloid plaques [11,18].

Our lab developed a sensitive liquid chromatography coupled to mass spectrometry technique for the analysis of GAGs in biological samples. By making use of fluorophore derivatization of unsaturated disaccharides with 2-aminoacridone (AMAC), this technique allows the detection and analysis of GAGs present even at low concentrations (picomole range) without the need for multiple enzymatic steps [19]. Several studies have demonstrated the robustness of this technique in analyzing samples of diverse biological origin, including cultured cells [20–22], decellularized structures [23–25] and biological fluids [26–28]. Of particular note, in our laboratory the GAG profile of NSCs differentiating on regular culture plates has been evaluated by Kim and co-worker using this method [29].

Several studies show the positive impact of scaffold properties (e.g., topography and electrical stimulation) on the differentiation of NSCs. This includes but are not limited to the incorporation of electroconductive/magnetic cues, cell-active moieties and small molecules/growth factors that can guide/fine-tune cell metabolism/differentiation [30–35]. However, to the best of our knowledge, there are no studies on the impact of topography on the GAG composition profile of NSCs. Therefore, the goal of this work was to evaluate GAG content changes on REN-VM cells, differentiating on electrospun nanofiber scaffolds. The results obtained here pave the way for a better understanding of GAG metabolism in NSCs during *in vitro* differentiation, critical for the optimization of tissue engineering strategies and for scaffold design as well as the discovery of new biomarkers for cell health.

2. Materials and methods

2.1. Materials

Poly(caprolactone) (PCL, MW 80,000), trifluoroethanol (TFE), poly(L-ornithine hydrobromide) (MW 30,000–70,000), glucose, human recombinant insulin, 2-(4-amidinophenyl)-6-indolecarbamidine dihydrochloride (DAPI), acetic acid, 2-aminoacridone (AMAC) and sodium cyanoborohydride ($NaBH_3CN$) were purchased from Sigma (St. Louis, MI). Medical glue (silastic® medical adhesive silicone type A) was obtained from Biesterfeld Spezialchemie Ibérica, SL (Barcelona, Spain). Ultra-low attachment 24-well plates (flat bottom) were obtained from Corning (Corning, NY). Dimethyl sulfoxide, methanol, and HPLC-grade water were purchased from Fisher Scientific (Hampton, NH). Trizma® hydrochloride, Dulbecco's phosphate buffer saline (DPBS), Dulbecco's Modified Eagle's Medium (DMEM-F12 + glutamax (1X)), Neurobasal medium, N2-supplement (100X), anti-anti mixture (penicillin 10,000 units/mL, streptomycin 10,000 μg/mL) human recombinant epidermal growth factor (EGF), human recombinant fibroblast growth factor 2 (FGF-2), B27-supplement (50X), reazurin (Alamar Blue® cell viability reagent), normal goat serum (10%), triton-x-100 (Surfact-Amps®, 10% in water), primary antibodies Anti-Tuj1 (mouse), Anti-GFAP (rat), Anti-MAP2 (mouse), secondary antibodies Alexa 488 anti-mouse, Alexa 546 anti-rat and Alexa 546 anti-rabbit, High-Capacity cDNA Reverse Transcription Kit, MicroAmp Fast Optical 96-well reaction plates and TaqMan® assays for SOX2 (Hs01053049_s1), Nestin (Hs04187831_g1), TUBB3 (Hs00801390_s1), GFAP (Hs00909233_m1), MAP2 (Hs00258900_m1), S100β (Hs00902901_m1) and GAPDH (Hs02786624_g1) were obtained from Thermofisher (Waltham, MA). Paraformaldehyde (PFA, 4% in phosphate buffered saline (PBS) was obtained from Alfa Aesar (Haverhill, MA). The primary antibodies Anti-Nestin (abc6320), Anti-SOX2 (abc92494) and Anti-S100β (abc868) were obtained from Abcam (Cambridge, UK). RNA extraction kit was purchased from Zymo scientific (Irvine, CA). The 17 unsaturated disaccharide standards of HS, CS and HA were purchased from Iduron (Aldery Edge, UK). 3K MWCO centrifuge columns were purchased from Millipore (Burlington, MA). Recombinant *Flavobacterial* heparinase I, II, III and chondroitin lyase ABC from *Proteus vulgaris* were expressed in our laboratory using *Escherichia coli* strains. A frozen stock of ReN-VM cells (Millipore – Burlington, MA) was used in these studies.

2.2. Polycaprolactone fibers production and characterization

PCL 13% (w/v) solution was prepared by mixing 1.3 g of PCL in 10 mL of TFE for 24 h. Electrospinning was performed using a spinneret system (MECC, Ogori, Fukuoka, Japan) (Fig. 1A) and a 23G needle (0.635 mm of internal diameter) under the following

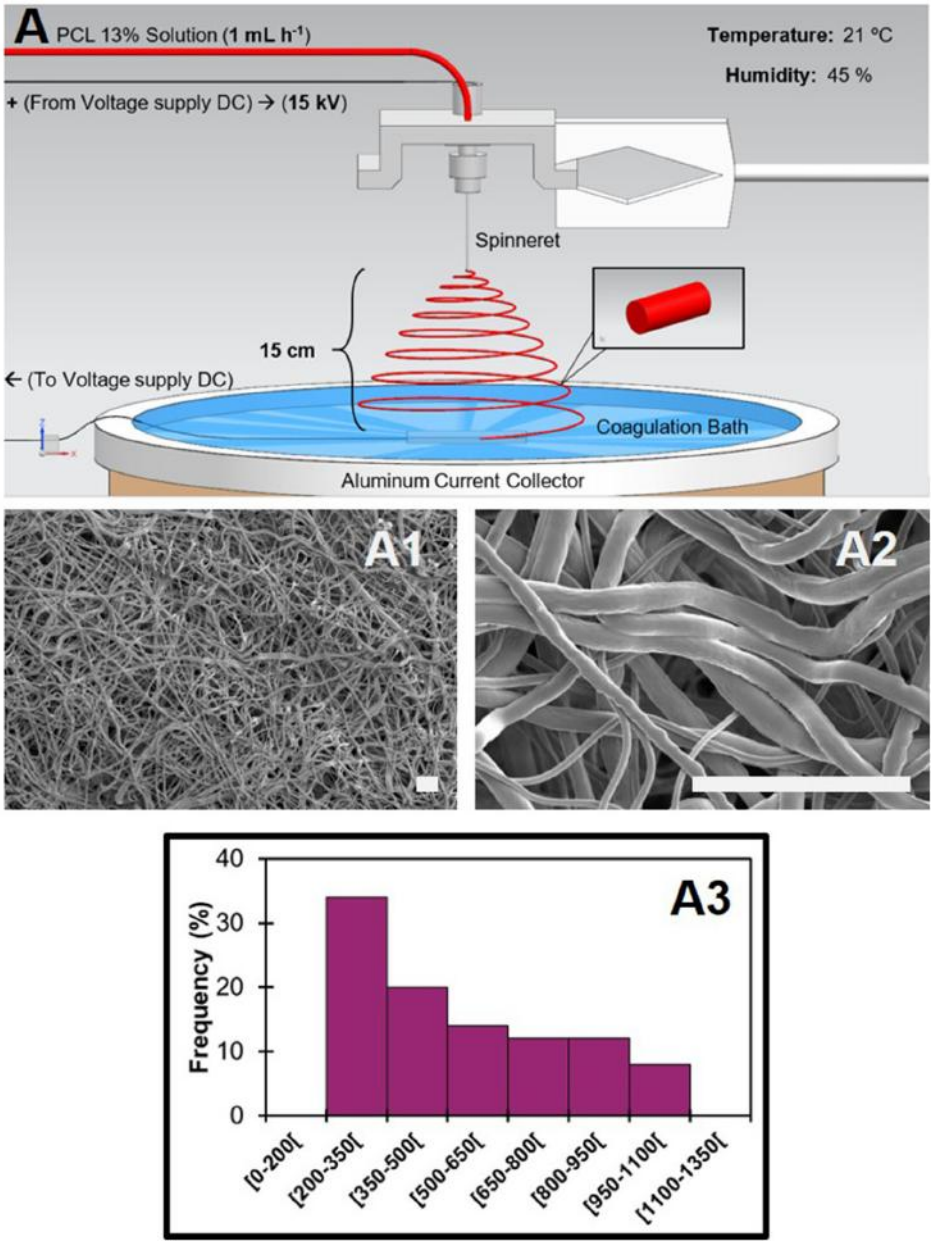

Fig. 1. (A) Schematics of the electrospinning setup used for the wet/wet production of monoaxial PCL fibers. SEM images of the wet-wet electrospun PCL fibers (A1, A2), and respective histograms for fiber diameter distribution (A3) (n = 50) (Scale bars = 10 μm).

conditions: voltage of 15 kV, flow rate at 30 μL min^{-1}, distance from needle to collector of 15 cm, temperature of 21 °C, relative humidity of 45%. Samples were collected on a water coagulation bath for complete TFE removal of the fibers and then dried under vacuum before further processing.

The morphology of the fiber mats obtained was evaluated using Scanning Electron Microscopy (SEM) (Carl Zeiss Supra 55 FESEM) at 1 kV, IL detector, after coating with a thin platinum layer. Fiber diameter was evaluated using SEM images. A total of 50 individual fibers for each combination were analyzed using NIH ImageJ software (National Institute of Health, MD, USA). The diameters obtained were averaged and the histogram was plotted using Microsoft Excel ®.

2.3. Neural stem cell proliferation and differentiation assays on the scaffolds

2.3.1. Cell culture

In this study the human-derived cell line REN-VM, NSCs immortalized through the transfection of c-myc, is used due to its ease of cell culturing and ability to differentiate into mature neural cells.

REN-VM were maintained as previously described [36]. Briefly, cells were grown on poly-ornithine (20 μg mL^{-1}, overnight) and laminin (10 μg mL^{-1}, 2 h) coated plates in N2 media, composed of DMEM/F12 with N2 supplement (1:100), additional glucose (1.6 g mL^{-1}), insulin (20 μg mL^{-1}) and pen-strep (1:100), and

supplemented with EGF (20 ng mL^{-1}), FGF-2 (20 ng mL^{-1}) and B27 (10 μL mL^{-1}), at 37 °C and 5% CO_2.

2.3.2. Scaffolds preparation

PCL fibers were glued to glass coverslips using medical glue for 24 h. Glass coverslips with medical glue added were used as the control. Samples were then collected and sterilized under UV radiation of 1.5 h per side and glued to a non-adherent plate overnight using medical glue at RT. Following this, sterilization with anti-anti 1% (in DPBS) solution was performed at 37 °C for 3 h before further processing.

2.3.3. Proliferation and differentiation assay

An adherent plate, glass coverslips and PCL fibers were coated with polyornithine (20 μg mL^{-1}, overnight) and laminin (10 μg mL^{-1}, 2 h) before being seeded with REN-VM cells (P10) (56,000 cells cm^{-2}). Supplemented N2 media was added 1.5 h after seeding (37 °C and 5% CO_2) to promote initial cell attachment.

On a first stage, cells were allowed to proliferate for 4 days on the scaffolds (proliferation phase – Fig. 2A). Media was exchanged at day 1, when cell adhesion was calculated, and then every two days. Cellular metabolic activity was assessed using Alamar Blue® at days 1, 2, 4 after cell seeding. Cell number was determined using a calibration curve (Fig. S1).

Cell differentiation assay (Fig. 2A) was adapted from Garrudo and co-workers [37]. Briefly, the assay was initiated at day 4 by changing the culture medium to N2B27 media, inducing spontaneous differentiation of REN-VM cells. N2B27 medium is composed of a 1:1 mixture of N2 medium (no growth factors added) and B27 medium. The B27 medium is composed of Neurobasal medium, B27 supplement (2:100), Glutamax (1:100) and pen-strep (1:200). Culture media was exchanged every two days until the end of the assay. Cellular metabolic activity was also assessed using Alamar Blue® on days 8 and 13 after seeding to evaluate the number of cells present on the fiber scaffolds.

2.4. Cell analysis

2.4.1. Immunofluorescence

After the differentiation assay, cells samples from days 4 (end of proliferation), 8 and 13 (end of differentiation) were fixed in PFA 4% for 10 min. They were then washed with DPBS twice and permeabilized with blocking solution (goat serum 10% and Triton-x-100 0.2% in DPBS) for 15 min at RT. After another washing step with DPBS, cells were incubated with Anti-MAP2 (1:200), Anti-S100β (1:200), Anti-Tuj1 (1:400), Anti-GFAP (1:250), Anti-Nestin (1:250) and Anti-SOX2 (1:100) diluted in staining solution (goat serum 5% and Triton-x-100 0.1% in DPBS) overnight at 4 °C. This was followed by incubation of the secondary antibodies Alexa 488 anti-mouse (1:250), Alexa 546 anti-rat (1:250) and Alexa 546 anti-rabbit (1:250) diluted in staining solution for 1 h at RT. Finally, DAPI (1 mg mL^{-1}) diluted in staining solution was added for 5 min at 37 °C. Cells were then washed, kept in DPBS and imaged using a confocal microscope (Zeiss LSM 510META Spectral Confocal). The image stacks obtained were then merged using ImageJ.

2.4.2. Quantitative polymerase chain reaction (Qpcr)

Quantitative real-time polymerase chain reaction (qPCR) was performed using TaqMan® gene expression assays. SOX2 (stem cells), Nestin (NSCs), TUBB3 (early neurons), GFAP (early

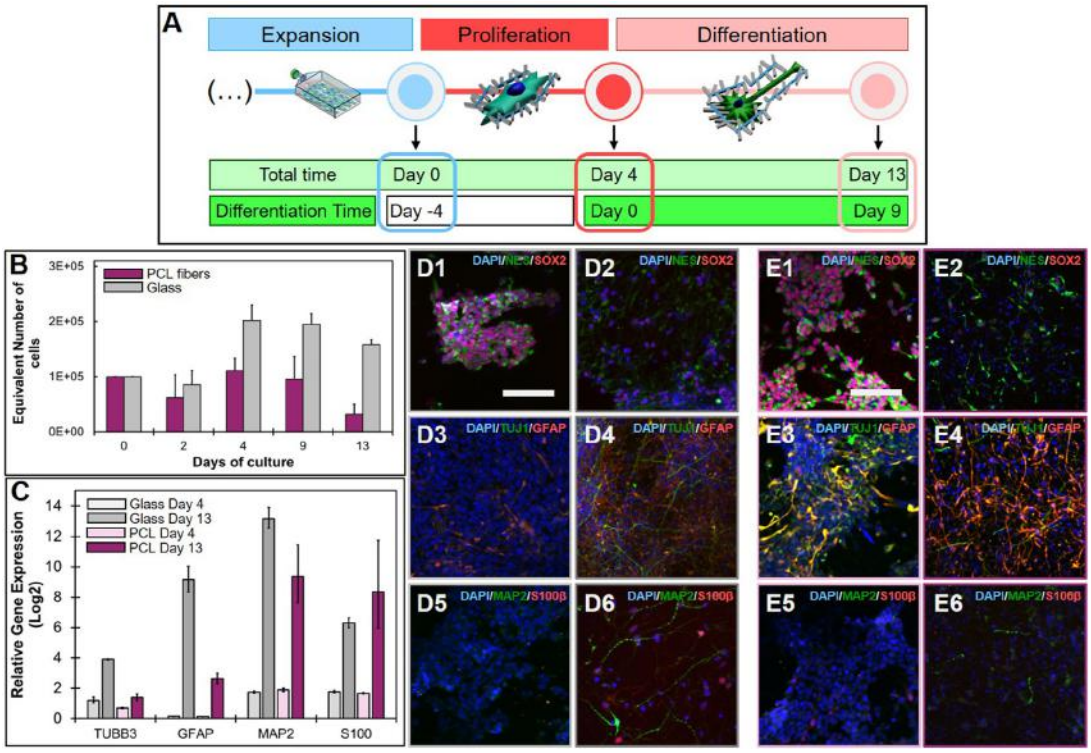

Fig. 2. (A) Summary of the cell culture protocol use in this work and respective timepoints. (B) Growth curve for ReN-VM cells growing Glass lamellas (grey) and PCL 13% fibers (dark pink) (mean ± std, n = 3). (C) qPCR analysis of the samples tested (mean ± sem, n = 2). (D,E) immunofluorescence analysis of ReN-VM cells growing on glass lamellas (D) and PCL 13% fibers (E) after 4 days of proliferation (Day 4) (D1, 3, 5 and E1, 3, 5) and 9 days of differentiation (Day 13) (D2, 4, 6 and E2, 4, 6) for different neural markers. All IF samples were counter-stained with DAPI (Blue) (Scale bar = 100 μm).

astrocytes), MAP2 (mature neurons) and S100β (mature astrocytes) were chosen as the main interest targets. Gene expression at days 4 and 13 (two independent samples per timepoint and condition) was determined using the comparative Ct method and by normalizing the expression of each target gene to the endogenous reference transcript GAPDH.

2.4.3. Gag profile analysis

2.4.3.1. Gag extraction and labbeling. Sample collection: Five independent cell samples from days 4 (end of proliferation) and 13 (end of differentiation) were collected from each condition tested, washed twice with DPBS and frozen until further processing. The corresponding culture media, collected together along the time of the experiment, was also frozen until further processing.

GAG extraction: For GAG extraction, fiber/glass lamellas samples containing the cells were directly sonicated using 100 μL of digestion buffer (BugBuster 10x protein extraction buffer) in an ice bath for 5 min per sample. The cell mixture and the cell culture media mixtures were then desalted using 3K MWCO centrifuge columns and the GAGs were collected for GAG lyase treatment.

GAG digestion: GAG samples from cells and culture media were treated with an enzyme mixture containing recombinant heparinase I, II and III, and chondroitinase ABC in digestion buffer (20 mU mg^{-1} of GAG in 50 mM ammonium acetate (NH_4CH_3COO) containing 2 mM calcium chloride ($CaCl_2$) adjusted to pH 7.0) at 37 °C for 6 h. The samples obtained were then cooled and centrifuged in 3 kDa spin columns to collect the disaccharide mixtures.

AMAC Labeling: Cell samples, culture media samples and the 17 standard disaccharide mixture were labeled using the following protocol: A 0.1 M AMAC solution was prepared by dissolving 0.21 mg of AMAC in dimethyl sulfoxide/acetic acid (17:3 v/v) and samples were incubated with 10 μL each for 5 min. Sodium cyanoborohydride (1 M, $NaBH_3CN$) solution was prepared by dissolving 6.28 mg of $NaBH_3CN$ in 100 μL of HPLC-grade water and samples were incubated with 10 μL each for 1 h at 45 °C. Samples were then centrifuged, and the supernatant was further analyzed by liquid chromatography-tandem mass spectrometry (LC-MS/MS).

2.4.3.2. Liquid-chromatography and double mass spectroscopy analysis (lc-Ms/Ms). LC–MS analyses were performed on an Agilent 1200 LC/MSD instrument (Agilent Technologies, Inc., Wilmington, DE) equipped with an Agilent Poroshell 120 ECC18 column (2.7 μm, 3.0 mm × 150 mm) at 45 °C and 90 bar. The flow rate was 300 μL min^{-1} and 5 μL of each sample per analysis were injected in the column. The mobile phases used were: 50 mM NH_4CH_3COO in water (A) and methanol (B): 5–45% B from 0 to 10 min, 45–100% B from 10 to 10.2 min, 100% B from 10.2 to 14 min, and 100 to 5% of B from 14 to 22 min. The detector used was a triple quadrupole mass spectrometry system equipped with an ESI source (Thermofisher Scientific, San Jose, CA). The MS analysis was done in the Multiple Reaction Monitoring (MRM) mode and the collected data was analyzed using the Thermo Xcalibur™ software (Thermofisher Scientific, San Jose, CA). Sample peaks were compared to ones obtained from external standards.

2.5. Statistical analysis

All data are presented as mean values ± standard deviations (SD). Statistical analysis was performed using Microsoft Excel. Significant differences between groups were measured using ANOVA test, followed by post-hoc analysis and Bonferroni correction. $p < 0.05$ was considered statistically significant.

3. Results and discussion

"Electrospun fibers have numerous advantages for neural tissue applications over flat substrates by providing support for neural stem cell adhesion and potentially enhance the differentiation of cultured NSCs [36,38–41]. In particular, random PCL fibers can be chemically modified to increase bioactivity [42] and their direct transplantation to the brain in vivo models not only avoids excessive scarring but also promotes neurite and cell infiltration [43] and a more complete neural cell integration of transplanted cells [5]. The aim of this work was to evaluate the effect of topography, induced by electrospun fibers, on both REN-VM differentiation and GAG profiles. This knowledge is critical not only for the smart design of better scaffolds for neural tissue engineering applications but also to understand the ECM dynamic of differentiating neural cells and to establish new biomarkers for disease progression. The first step in this study aimed at the selection of the appropriate platform for neural cell proliferation and differentiation. PCL is a biocompatible and biodegradable polymer that is approved by the US food and drug administration (FDA) for food packing and medical devices such as sutures, materials for craniofacial applications and resorbable devices for peripheral nerve repair [44–46]. Moreover, PCL is easy to electrospun and several different scaffolds have been developed and studied for neural applications in the past years [30,36,47–49]. As such, monoaxial PCL nanofibers were successfully obtained and used for these studies. SEM images and the respective histogram of the fibers diameter distribution are presented in Fig. 1 (A1-3). Their average diameter was 543 ± 267 nm.

REN-VM cells were seeded on PCL fibers and glass lamellas (control) to study the effect of topography on their differentiation profile, which included their GAG profile. The general cell culture protocol can be found in Fig. 2A The variation in cell number can be seen in Fig. 2B, indicating that after 4 days of proliferation cell number was the highest, but decreased until the end of the experiment. The success in the differentiation protocol was evaluated through both immunofluorescence and qPCR assays and the following neural markers were used: sex determining region Y-box 2 (SOX2) for stem cell phenotype; the type VI intermediate filament nestin (NES) for neural ectodermal phenotype; neuron-specific class-III beta-tubulin (Tuj1) for early neuron phenotype; glial fibrillary acidic protein (GFAP) for early astrocyte phenotype; microtubule-associated protein 2 (MAP2) for intermediate neuron phenotype; and S100 calcium-binding protein B (S100β) for mature astrocyte phenotype.

qPCR analysis of the differentiated REN-VM cells (Fig. 2C) revealed changes in gene expression, namely an increase in the markers for both neurons (TUBB3 and MAP2) and astrocytes (GFAP, S100β). ANOVA analysis indicated the presence of statistically significant increases in GFAP and MAP2 during differentiation, but not in TUBB3 and S100β. However, a post-hoc test used did not allowed to identify where these differences occurred. Complementary immunofluorescence (Fig. 2D and E) analysis allowed the identification of these same markers on differentiated cells (day 13 samples) on both glass lamellas and PCL fibers. As expected, the morphology of differentiating REN-CM cells changes from a spindle/stellar morphology (day 4 samples) to a more elongated one (day 13 samples), similar to what is observed in neurons and astrocytes [50,51]. NES and SOX2 were still present in differentiated cells but their fluorescence intensity was reduced in all the samples. Finally, both neural markers Tuj1 and MAP2 and both astrocytic markers GFAP and S100β were present at higher levels in differentiated cells than in undifferentiated ones. Overall, our results support the successful differentiation of REN-VM cells on both scaffolds used.

The coexistence of non-differentiation (SOX2, NES) and

differentiation markers (Tuj1, GFAP, MAP2, S100β) simultaneously in REN-VM cells (Fig. 2D and E) is intriguing. SOX2 is one of the major factors used to reprogram fibroblasts into induced pluripotent stem cells (iPSCs) [52,53]. In the CNS, SOX2 is majorly expressed in NSCs and its expression decreases when neural differentiation occurs [54,55]. REN-VM cells were engineered to overexpress the oncogene *c*-myc. As a result, when REN-VM cells are exposed to the growth factor FGF-2 the *c-myc* gene is activated and triggers the production of SOX2 [56]. The increase in SOX2 levels in REN-VM cells leads to the activation of several genes including NES and cyclin dependent kinases, promoting cell cycle progression [57,58]. This overexpression of c-myc can be responsible for the presence of SOX2 and NES in our cell population throughout proliferation but cannot explain its persistence during differentiation. Ng and co-workers report that SOX2 expression is a key element for REN-VM cell differentiation through interaction with the long noncoding RNA rhabdomyosarcoma 2-associated transcript (RMST), and therefore can be important in an early differentiation stage [54]. We hypothesize that when FGF2 is withdrawn from the culture medium differentiation occurs but SOX2 expression persists and promotes NES expression, which might explain its persistence in the cells after differentiation (day 13 samples).

Overall, the immunofluorescence and qPCR results obtained show REN-VM cells able to grow and differentiate on both glass lamellas and PCL fibers. The next step was to investigate changes in the GAG profile during cell growth and differentiation. The general protocol for sample collection and preparation, along with the involved AMAC labeling reactions and the used standards profile obtained are shown in Fig. 3. The composition of each of the GAGs analyzed is presented in Table 1. A preliminary assessment of the GAG profile of differentiating REN-VM cells growing and differentiating on culture plates was performed and these suggest differences between the undifferentiated and differentiated cells (Fig. S2). These are in line with the observations made by Kim and co-workers [29] who report high levels of HS and low levels of CS and HA in the cell samples analyzed.

After sample collection and GAG digestion the disaccharides obtained were labeled with AMAC and analyzed by LC-MS for identification. Cell samples were first analyzed (Fig. 4A, Fig. 5 and Table 2). Because the collection method involved the physical and chemical digestion of the cells attached to each of the scaffolds, these contain both REN-VM cells and the deposited ECM. For the original cell pellet (REN-VM cells), the total GAG profile (Fig. 4A, purple bars) shows a predominance of HS (54%) over CS (34%) and HA (12%). Both glass lamellas (grey bars) and PCL (pink bars) grown/differentiated samples have slightly higher HS content (both not statistically significant different), similar CS content and lower HA content compared to the pellet.

Kim and co-workers [29] report the production of higher amounts of HA by undifferentiated REN-VM cells (14.5%) than the amount obtained in this work (1.6% for glass lamella and 4.9% for PCL) for the equivalent cell culture period, i.e. after 4 days of cell

Table 1
Composition of the disaccharides analyzed through LC-MS/MS. ΔUA correspond to unsaturated uronic acid derivatives, which were AMAC-labeled.

CS disaccharides	
TriSCS	ΔUA2S(1,3)GalNAc4S6S
2S4SCS	ΔUA2S(1,3)GalNAc4S
2S6SCS	ΔUA2S(1,3)GalNAc6S
4S6SCS	ΔUA(1,3)GalNAc4S6S
2SCS	ΔUA2S(1,3)GalNAc
4SCS	ΔUA(1,3)GalNAc4S
6SCS	ΔUA(1,3)GalNAc6S
0SCS	ΔUA(1,3)GalNAc
HS disaccharides	
TriSHS	ΔUA2S(1,4)GlcNS6S
NS6SHS	ΔUA(1,4)GlcNS6S
NS2SHS	ΔUA2S(1,4)GlcNS
NSHS	ΔUA(1,4)GlcNS
2S6SHS	ΔUA2S(1,4)GlcNAc6S
6SHS	ΔUA(1,4)GlcNAc6S
2SHS	ΔUA2S(1,4)GlcNAc
0SHS	ΔUA(1,4)GlcNAc
HA disaccharide	
OSHA	ΔUA(1,3)GlcNAc

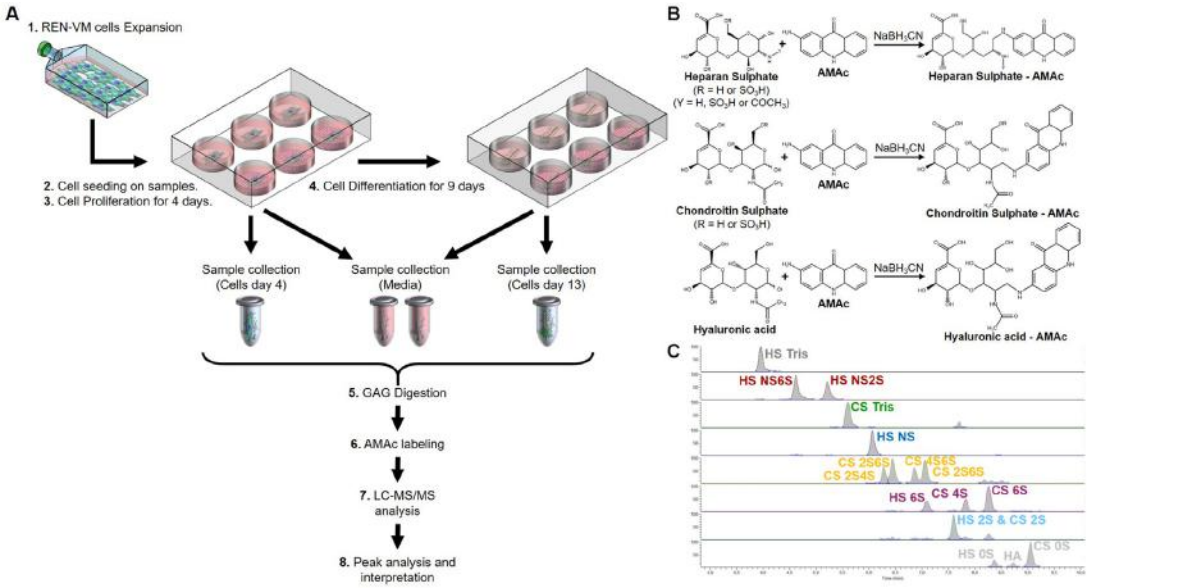

Fig. 3. (A) General workflow for the GAG analysis of REN-VM samples differentiated on glass lamellas or PCL fibers using the LC-MS/MS method. (B) AMAC labeling reactions performed for the different GAGs analyzed. (C) General profile of the original GAG standards used in the analysis.

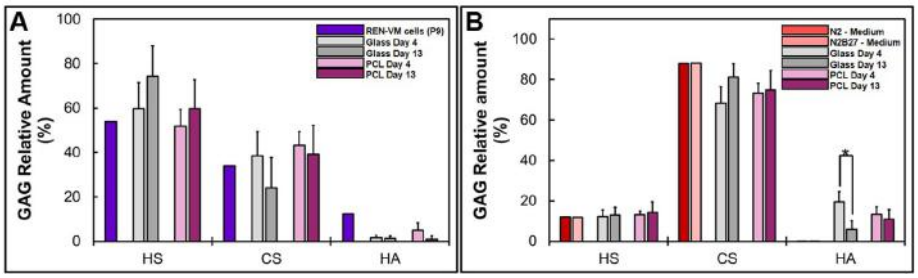

Fig. 4. Total GAG composition for (A) cell and (B) culture media samples (mean ± std, n = 5).

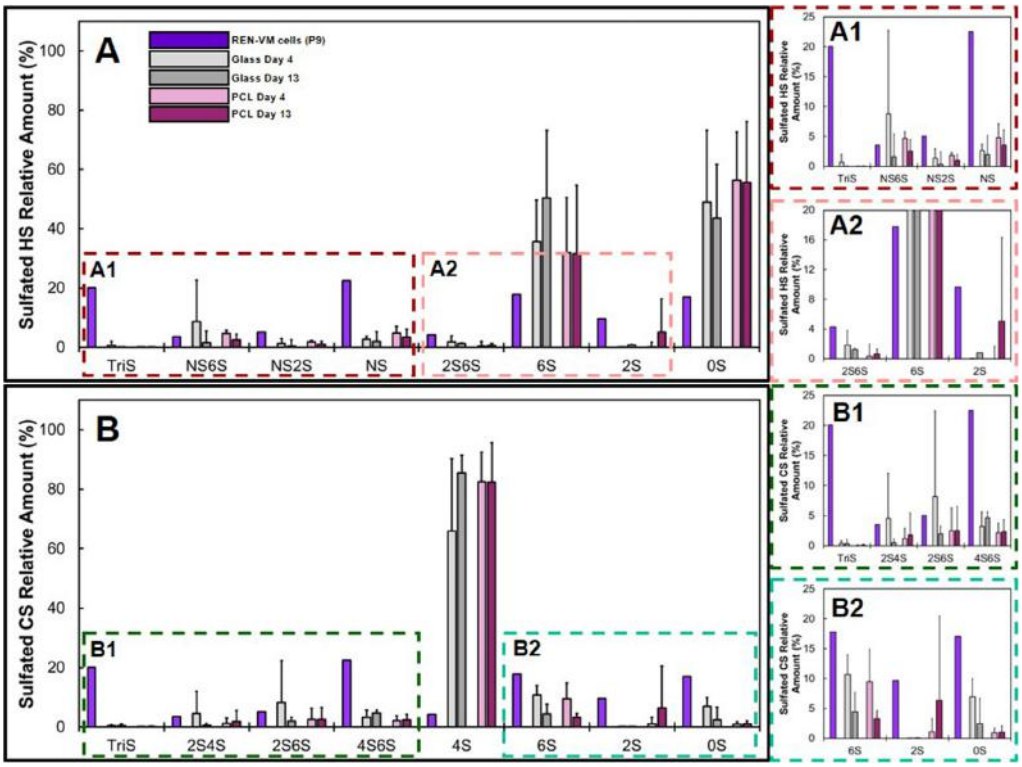

Fig. 5. GAG profile for cell samples. (A) Sulfated HS profile and respective close-ups (A1, A2). (B) Sulfated CS profile and respective close-ups (B1, B2) (mean ± std, n = 5).

proliferation. A similar trend was also observed for HA production after cells differentiation, which value reported by Kim and co-workers was 4.05% after two weeks of differentiation and, in the current study, 1.3% for glass lamellas and 1.0% for PCL after 9 days of differentiation (i.e. after 13 days of cell culture). Differences were also found regarding the HS and CS content of all our samples. In particular, cell samples cultured on PCL and Glass were consistently found to produce higher total CS values when compared to Kim and co-workers undifferentiated (5.1%), 2-week differentiated (5.9%) and 4-week differentiated (10.1%) samples. Conversely, HS values for the same samples (Table 2) were found to be lower (80.5% for undifferentiated, 85.5% for 2-week differentiated and 74.2% for 4-week differentiated).

CS is an important neural ECM component, namely due to its presence in perineural networks that naturally maintain synapse integrity in neural cells [59,60]. The higher values of CS found in the samples obtained point to the formation of a more mature ECM by cultured REN-VM cells in both substrates tested. Several hypothesis can be considered to explain such differences, being the first one the substrate used. First, we excluded a possible contamination with culture media since all cell samples were washed with DPBS prior to GAG extraction. Next, when we compared the cell culture protocol used three main differences were found: the culture medium (commercial REN-VM maintenance medium); the cell substrate (culture plate); and the duration of the differentiation process (2 and 4 weeks). In this work we used N2 medium, supplemented with EGF and FGF, for the proliferation phase and N2B27 medium for inducing spontaneous differentiation of REN-VM cells, which combines the optimal cell differentiation properties of N2-medium and the neural support properties of B27-media [61]. The formulation of the commercial medium used by Kim and co-worker is not available, and therefore we cannot compare their composition. Finally, because the CS/HS composition of REN-VM cells original pellet is similar to the values obtained for PCL and Glass samples, we hypothesize the culture media to be the main explanation for the different values observed.

Singh and Bachhawat [13] report the composition of GAGs present in the adult human brain to be 35% of HA, 34% of the sulfated CS (85% of CS4S and CS6S), 9.4% of low sulfated CS, 6% of HS, 5% of dermatan sulfate and the remaining are unidentified GAGs. The authors suggested that the relative composition of CS4S/CS6S varies during development since it is associated with neural plasticity. For example, it is reported that the relative proportion of CS4S to CS6S in the Neonate is 66%–34%, respectively, and the amount of CS6S decreases in children (16%) and again in adults (13%) with a proportional increase in CS4S. This corresponds to different CS4S/CS6S ratios for neonates (1.94), children (5.13) and adults (6.50). The cell samples studied here show CS4S/CS6S ratios similar or higher to the one reported for adults. Namely, glass day 4 and day 13 samples have ratios of 6.17 and 19.4, respectively, while PCL day 4 and day 13 have ratios of 8.7 and 25.0, respectively. The original REN-VM cells have a ratio of 1.95, closer to the one found in neonates. These values indicate that undifferentiated (day 4 samples) and differentiated (day 13 samples) REN-VM cells have a GAG content compatible with a less plastic environment as found in the human brain. Kim and co-workers [29] report a similar trend for undifferentiated and 2-week differentiated REN-VM cells. Moreover, in their study CS6S content is shown to drastically increase compared to CS4S after 4 weeks of differentiation. An explanation for this observation is a possible role of CS4S in the initial confinement of NSCs, similar to what happens during the development of the neuroepithelium in chick [62]. This might indicate that both glass and electrospun PCL nanofibrous platforms, used to compare NSC differentiation, might not influence the process in the timeframe of this experiment. However, it is possible that more drastic changes are seen for longer differentiation protocols.

Changes regarding the sulfated CS profile of the cell samples (Fig. 5 B, B1 and B2) are also observed in cell samples. Comparing the CS sulfated disaccharides from the cell pellet with cell samples showed higher levels of CS4S, as observed by Flangea and co-workers for mice [63], and lower levels of the remaining forms (TrisS, 2S4S, 2S6S, 4S6S, 6S, 2S and 0S), with no differences observed between days 4 (undifferentiated) and 13 (differentiated). Their role in brain tissue is to regulate the growth, migration of neural cells and dendritic/axonal guidance. Interestingly, CS4S is a major component of proteoglycans present in perineural networks, a specialized ECM system that develops around parvalbumin positive GABAergic neurons. CS4S together with CS6S are two of the more studied disaccharides present in perineural networks. When enriched in one of these two disaccharides, proteoglycans can either inhibit or promote axon growth and guide its direction [14]. As an example, in the work of Erskine and co-worker the application of electrical current (50–133 mV mm^{-1}) to *Xenopus sp.* nerve cells with culture medium supplemented with glycosaminoglycans enriched in either with CS4S or CS6S produced distinctive effects on cells. At the highest electrical fields tested (133 mV mm^{-1}) when CS6S enriched GAGs were added, dendrites sprouted to the cathode, following the direction of the electrical field, whereas when CS4S enriched GAGs were added neurite formation was inhibited. Another interesting observation of the study of Erskine and co-workers was that the structure of the GAGs used was directly associated to the effects observed and supplementation with the resulting digested disaccharide units did not produced the same effects [64]. This effect can be related to the ability of sulfated GAGs to bind to active molecules, such as the case of the specific bond of semaphoring 3A to CS4S6S [14,65]. In our work, the CS4S and CS6S values for both samples are similar, indicating that both substrates can potentiate axonal/dendrite growth similarly. Contrary to Kim and co-workers the long-term effect (4 weeks of differentiation) of culture on both substrates was not performed, and therefore the long-term effects on CS4S/CS6S ratio should be evaluated in future works.

Changes regarding the sulfated HS profile of the cell samples (Fig. 5 A, A1 and A2) are observed. Compared with the original cell pellet, higher amounts of HSNS6S, HS6S and HS0S and lower amounts of TriS, HS2S6S, HSNS and HS2S were observed. No significant statistical differences were found between days 4 and 13 samples. Nevertheless, the results obtained show that regardless of the type of cell culture platform used, neural cells were able to express important sulfated HS components. For example, HS6S together with HS2S is important for neural cells patterning and axon migration. Also, during the development of the eye HS2S is necessary to signal neuron organization into bundles, whereas HS6S is necessary to keep neuron projections on track in the optic nerve and chiasm [59]. The role of the remaining GAGs in neural cell metabolism and differentiation remains to be fully understood.

Cell culture medium samples (Figs. 4B and 6 and Table 2) were analyzed to search for soluble GAGs. These are cumulative samples, where every aliquot of medium collected throughout media change from cultured cells, were saved together. To account for potential

Table 2
Disaccharide analysis for REN-VM cell culture medium and cell pellet samples.

Disaccharides	CULTURE MEDIUM SAMPLES						CELL PELLET SAMPLES				
	N2 Medium	N2B27 Medium	Glass Day 4	Glass Day 13	PCL Day 4	PCL Day 13	REN-VM (P9)	Glass Day 4	Glass Day 13	PCL Day 4	PCL Day 13
Total HS	12	11.8	12.2 ± 3.4	12.9 ± 3.9	13.1 ± 1.9	14.2 ± 5.4	53.9	59.8 ± 11.6	74.4 ± 13.6	51.8 ± 7.6	59.8 ± 13.0
TriS	0.0	0.0	0.0 ± 0.0	0.0 ± 0.0	0.0 ± 0.0	0.0 ± 0.0	20.1	0.7 ± 1.4	0.0 ± 0.0	0.1 ± 0.0	0.1 ± 0.1
NS6S	0.1	0.3	2.0 ± 1.1	3.0 ± 3.0	0.7 ± 0.2	1.2 ± 0.5	3.5	8.7 ± 14.0	4.7 ± 3.8	1.6 ± 1.1	2.6 ± 1.9
NS2S	0.1	0.1	0.2 ± 0.2	0.4 ± 0.2	0.2 ± 0.1	0.6 ± 0.5	5.1	1.4 ± 1.6	1.9 ± 2.1	0.4 ± 0.4	1.0 ± 1.0
NS	0.2	5.3	2.1 ± 2.0	4.5 ± 7.2	1.6 ± 1.7	4.3 ± 1.0	22.5	2.7 ± 1.0	4.8 ± 3.2	2.0 ± 2.4	3.5 ± 2.6
2S6S	0.2	0.1	0.1 ± 0.0	0.4 ± 0.5	0.1 ± 0.1	0.7 ± 0.7	4.3	1.8 ± 2.0	0.3 ± 0.2	1.2 ± 1.7	0.6 ± 0.7
6S	3.2	1.5	5.0 ± 3.0	2.3 ± 1.9	9.7 ± 15.0	3.6 ± 1.5	17.8	35.7 ± 14.0	32.0 ± 22.9	50.3 ± 18.6	31.5 ± 23.2
2S	0.1	1.6	0.0 ± 0.0	0.1 ± 0.1	0.2 ± 0.4	0.1 ± 0.1	9.7	0.0 ± 0.1	0.0 ± 0.0	0.8 ± 1.7	5.1 ± 11.2
0S	96.1	91.0	90.5 ± 3.08	89.3 ± 9.9	87.6 ± 16.1	89.5 ± 2.2	17.1	49.0 ± 24.3	56.3 ± 18.1	43.6 ± 16.3	55.6 ± 20.6
Total CS	88	88.2	68.2 ± 8.1	81.3 ± 6.3	73.5 ± 4.8	74.9 ± 9.5	33.8	38.6 ± 10.9	24.3 ± 13.5	43.3 ± 6.2	39.3 ± 13.0
TriS	0.0	0.0	0.0 ± 0.0	0.0 ± 0.0	0.0 ± 0.0	0.0 ± 0.1	12.1	0.4 ± 0.4	0.4 ± 0.7	0.1 ± 0.1	0.1 ± 0.2
2S4S	0.0	0.1	0.1 ± 0.0	0.1 ± 0.1	0.1 ± 0.0	0.1 ± 0.1	9.9	4.5 ± 7.5	0.5 ± 0.7	1.2 ± 1.7	1.8 ± 3.6
2S6S	0.1	0.3	0.2 ± 0.2	0.1 ± 0.1	0.2 ± 0.1	0.2 ± 0.1	10.6	8.2 ± 14.2	2.0 ± 1.3	2.5 ± 3.8	2.5 ± 4.0
4S6S	1.6	1.9	3.5 ± 0.8	2.7 ± 0.7	3.3 ± 0.5	3.6 ± 0.4	5.9	3.2 ± 2.4	4.6 ± 1.0	2.1 ± 1.6	2.4 ± 1.9
4S	96.9	96.0	92.2 ± 1.6	93.9 ± 1.5	92.5 ± 1.3	93.1 ± 1.1	26.4	66.0 ± 24.3	85.5 ± 6.0	82.6 ± 9.9	82.5 ± 13.3
6S	1.2	1.5	3.7 ± 1.6	2.4 ± 1.6	3.7 ± 1.6	2.9 ± 1.6	13.3	10.7 ± 3.3	4.4 ± 3.3	9.5 ± 5.4	3.3 ± 1.4
2S	0.0	0.2	0.0 ± 0.0	0.0 ± 0.0	0.0 ± 0.1	0.0 ± 0.0	15.4	0.1 ± 0.1	0.1 ± 0.1	1.1 ± 2.2	6.4 ± 14.1
0S	0.2	0.0	0.2 ± 0.2	0.6 ± 0.1	0.3 ± 0.3	0.1 ± 0.1	6.4	6.9 ± 3.0	2.5 ± 4.2	0.9 ± 0.8	1.0 ± 1.0
Total HA	0.0	0.0	19.6 ± 5.0	5.8 ± 4.1	13.4 ± 3.5	10.9 ± 4.7	12.3	1.6 ± 1.1	1.3 ± 1.1	4.9 ± 3.4	1.0 ± 1.5

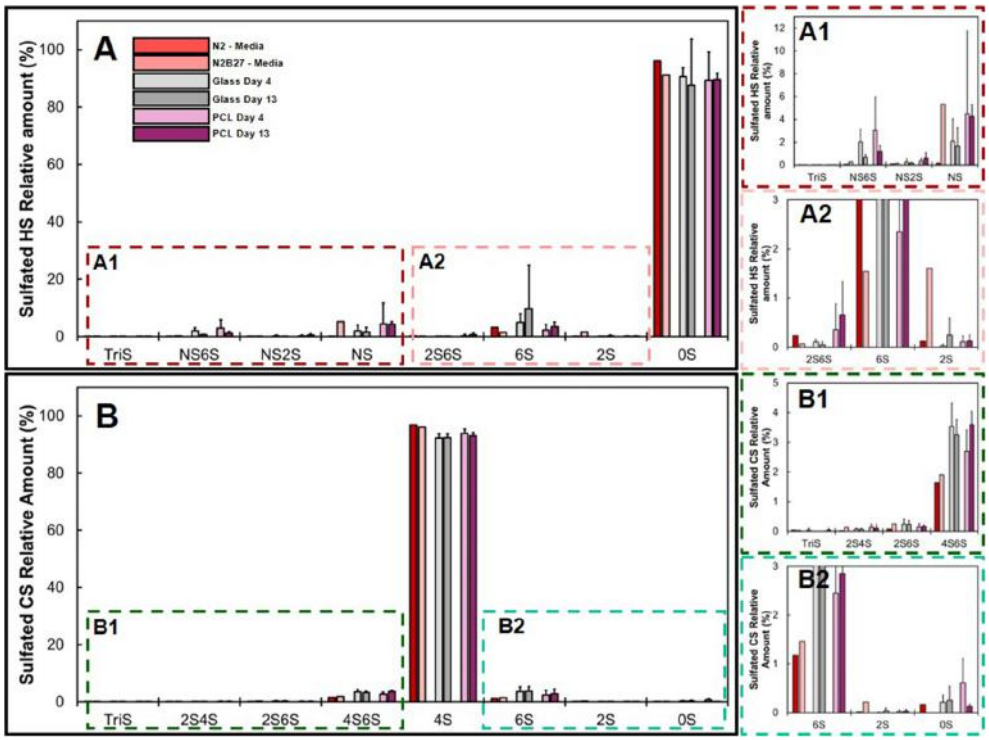

Fig. 6. GAG profile for culture medium samples. (A) Sulfated HS profile and respective close-ups (A1, A2). (B) Sulfated CS profile and respective close-ups (B1, B2) (mean ± std, n = 5).

contribution of cell culture media components to GAG quantification, it was analyzed the original formulation of both N2 and N2B27 medium used for the proliferation and differentiation phases respectively. The major component of both media is CS (90% for N2 and 87% for N2B27), followed by HS (10% for N2 and 13% for N2B27). With regards to sulfated HS disaccharides, only HS0S (99.9%) is found in both formulations. In the case of sulfated CS forms, CS4S is the major component (96.7% for N2 and 95.1% for N2B27) followed by CS4S6S (1.8% for N2 and 3% for N2B27) and CS6S (1.2% for N2 and 1.4% for N2B27).

The total GAG profile (Fig. 4B) of the culture media collected is very similar to the profiles of N2- and N2B27-media. The major difference observable was in HA content, which is not found in the fresh culture media samples. A significant statistical difference in HA was found between days 4 and 13 for cells cultured on glass lamellas. Regarding the sulfated HS profile (Fig. 6 A, A1 and A2), a higher amount of HS6S (mostly undetected in the fresh culture media samples) was found on culture media exposed to cell culture. Again, for the sulfated CS profile (Fig. 6 B, B1 and B2) no major differences are observed among the samples. However, higher amounts of CS4S6S, CS6S and CS0S were found in the spent cell culture medias. Apart from HA, no major GAG content changes were observed between different cell cultured samples of differentiating REN-VM cells.

The presence of HA in the spent culture media samples is intriguing. HA is a key component of neural ECMs, constituting a binding partner to several neural proteoglycans such as neurocan, aggrecan and versican [60]. The amount of HA changes during development. In young rats, 90% of the HA present is removable by water, contrasting with the 15% obtained in adult rats [66]. This higher amount of water-soluble HA is responsible for the increased water content in young rats brains and is proposed to facilitate cell migration during brain development. When found in the grey matter, HA is present in perineural networks for supporting long-range neurons, whereas in the white matter HA is found ubiquitously. HA is not present in the fresh culture media GAG composition, and its presence can only be attributed to cell activity. It is possible that REN-VM cells express high levels of hyaluronidases and the presence of HA in the media might be a consequence of the natural ECM remodeling mechanism [67,68].

There are two different types of HA, high molecular weight HA (HMWHA) (>1000 kDa), capable of maintaining cells quiescence and preventing cell maturation, and low molecular weight HA (LMWHA) (<30 kDa), which can trigger NSC proliferation and retard differentiation [69,70]. The HA detected in the culture media, possibly corresponding to LMWHA, can be associated with cell membrane hyaluronidase activity and ECM production by the cells in both glass and PCL samples. The relative amount of HA decreases in glass samples from day 4 to day 13, which was accompanied by an increase in CS (Fig. 4B). This might indicate a possible decrease in the production of LMWHA due to a shift in the cell's metabolism and the production of a more mature neural ECM [71]. In spent cell culture media samples, obtained from PCL fibrous scaffolds, no such changes were observed and the relative disaccharide composition remain stable. However, higher amounts of soluble HA were detected.

Other disaccharides found in the spent cell media and not present in the initial fresh culture media included HS6S, CS4S6S, CS6S and CS0S. HS disaccharides are present in numerous cell adhesion proteins, including syndecans and glypicans [72]. HS6S along with HS2S are important for correct neural guidance in the optic chiasm of mice, the migration of different cells in the hindbrain and for controlling the signaling pathway of FGF2, so their identification in the culture media is intriguing. The presence of HS6S in the culture

media might indicate the presence of cellular debris from cell death or exosomes or ECM debris from the turnover of the ECM synthesized by REN-VM cells. CS derived proteoglycans are primarily present in ECM and, therefore, the presence of CS4S6S, CS6S and CS0S might also be explained by the presence of ECM debris from the turnover of the ECM by REN-VM cells.

Electrospun fibers present numerous important advantages for tissue engineering application, namely in the design and construction of adequate biomaterials. They are 1) able to mimic the natural extracellular matrix present in tissues, which creates nano-topographical cues that favor neural cell proliferation/differentiation [38,73,74]; 2) provide high surface area, which can promote cell adhesion [75]; 3) can be made of either natural and/or synthetic materials and their properties can be finetuned to the tissue requirements to boost biocompatibility [76]; and 4) their bioactivity can be enhanced by the immobilization of biomolecules [42,77]. Our work demonstrates for the first time that substrate topography of PCL fibers can also influence the production of GAGs present in the ECM. We show that cells generate an ECM enriched in CS, a major component of neural ECM, when cultured on PCL fibers, but that no differences were found in their sulfation profile. Moreover, higher amounts of HA, possibly LMW-HA, are found in the spent culture media of proliferating (day 4) and differentiating (day 13) REN-VM cells when cultured on PCL fibers. We conclude that REN-VM cells, when cultured on PCL fibers, produce a more neural-friendly ECM, similar to that present in the neural tissue [13]. We suggest that the superiority of electrospun-based substrates (PCL fibers) over flat substrates (glass coverslips) is also associated with the production of a more plastic and dynamic ECM, more suitable for tissue engineering applications [78–80]. This factor might explain, after PCL fibers transplantation into rats, the limited tissue scar formation and increased neurite penetration on PCL observed by Nisbet and colleagues [43], and the enhancement of transplanted induced neural cells into mice brain tissue, observed by Carlson and colleagues [5] when such cells were cultured on electrospun fibers.

In summary, changes occurred in the amount of HS and HA present in differentiating REN-VM cells cultured on lamellas and PCL nanofibers but no changes in major sulfated GAG content were observed in the remaining disaccharides that were analyzed. With the observations of this work we can also suggest some recommendations for the construction of scaffolds for neural tissue engineering. First, HA is a good candidate material to use but a balance must be struck between the amount of LMWHA and HMWHA so as not to compromise either proliferation or differentiation. In the case of HS and CS GAGs, CS should be the best candidate for scaffold functionalization since it is naturally present in the spent culture media and in the synthesized ECM. Other strategies such as using bio-inks with GAGs enriched with certain disaccharides (CS4S or CS6S) might also be applied to create bioactive scaffolds. This is especially important for diseases that require scaffolds to mimic the complex architecture of the original tissue or if cell migration is desired in a certain direction. Moreover, additional improvements in the methodology used are necessary to allow the analysis of keratan sulfate, another important component of CNS GAGs. Finally, additional studies need to be conducted to determine the effect of other topographic and/or three-dimensional structures on neural cell differentiation and correspondent GAG profile. Importantly, other cells types, such as induced pluripotent stem cells (iPSCs) might be more suitable candidates since they are not an immortalized line and can recapitulate normal neural cell development.

4. Conclusions

PCL 13% nanofibers, obtained by wet/wet electrospinning, allowed consistent REN-VM cell growth and differentiation. Cells growing and differentiating on both glass lamellas and PCL nanofibers afforded similar disaccharide profiles. Nevertheless, we found cells generate an ECM enriched with CS when cultured on PCL fibers, and no differences were found in their sulfation profile. Higher amounts of HA, possibly LMW-HA, were also found in the spent culture media of proliferating (day 4) and differentiating (day 13) REN-VM cells when cultured on PCL fibers. The information obtained in this work can be used to improve the design of, for example, electroconductive scaffolds for neural tissue engineering applications. These will be important not only for the development of *in vitro* platforms to study disease mechanisms and to test new drugs but also for the development of smart and more effective tissue-engineered implants for transplantation into patients afflicted with neurological diseases.

Author contribution

Original idea: FFFG and PEM. Experimental plan: FFFG, PEM, and RJL. Preliminary results: FFFG, CAVR and YY. Electrospun and cell work experiments: FFFG, assisted by CAC and PRH. GAG analysis: KX, YO, XH, FFFG and CAC. Data analysis: FFFG, PEM and JCS. Laboratory space and funding: JMSC, JM, FCF and RJL. Manuscript writing: FFFG and RJL. All authors revised the manuscript.

Declaration of competing interest

The authors declare that they have no known competing financial interests or personal relationships that could have appeared to influence the work reported in this paper.

Acknowledgements

All authors thank the support from the Center for Biotechnology & Interdisciplinary Studies (CBIS) and the Center for Materials, Devices, and Integrated Systems (CMDIS). The authors are also thankful to Dr. Dmitri Zagorevski for LC-MS assistance. Finally, a special thanks to Dr. So-Young Kim and Dr. Gregory Nierod for discussing the experimental plan, to Dr. Johnathan Dordick for providing the REN-VM cells and to both Charles Willard and Dr. Ranodhi Udangawa Keating for the electrospinning setup figure used.

Appendix A. Supplementary data

Supplementary data to this article can be found online at https://doi.org/10.1016/j.biochi.2021.01.001.

Funding

This work is funded by the US National Institutes of Health, grant # DK111958 and New York State grant # SCRIB DOH01-PART2-2017. Other funding included: iBB - Institute for Bioengineering and Biosciences from FCT - Portuguese Funding for Science and Technology (UID/BIO/04565/2020), Programa Operacional Regional (POR) de Lisboa 2020 (Project N. 007317), POR de Lisboa 2020 through the project PRECISE - Accelerating progress toward the new era of precision medicine (Project N. 16394) and the project NEURON, PTDC/CTM-CTM/30237/2017 also from FCT.

Finally, FFFG and JCS acknowledge FCT for the PhD scholarships PD/BD/114045/2015 and SFRH/BD/105771/2014 respectively.

References

[1] Global of Collaborators, Global, Regional, and National Burden of Neurological Disorders, 1990–2016: a Systematic Analysis for the Global Burden of Disease Study 2016, 2019.

[2] M. Erkkinen, M.-O. Kim, M. Geschwind, Clinical neurology and epidemiology of the major neurodegenerative diseases, Csh Perspect. Biol. 10 (2018), a033118.

[3] C.-H. Chou, H.-C. Fan, D.-Y. Hueng, Potential of neural stem cell-based therapy for Parkinson's disease, Park S Dis. (2015) 1–9, 2015.

[4] L. Tian, M.P. Prabhakaran, J. Hu, M. Chen, F. Besenbacher, S. Ramakrishna, Synergistic effect of topography, surface chemistry and conductivity of the electrospun nanofibrous scaffold on cellular response of PC12 cells, Colloids Surf., B 145 (2016) 420–429.

[5] A. Carlson, N. Bennett, N. Francis, A. Halikere, S. Clarke, J. Moore, et al., Generation and transplantation of reprogrammed human neurons in the brain using 3D microtopographic scaffolds, Nat. Commun. 7 (2016), 10862.

[6] W. Chen, Q. Huang, S. Ma, M. Li, Progress in dopaminergic cell replacement and regenerative strategies for Parkinson's disease, ACS Chem. Neurosci. 10 (2019) 839–851.

[7] D. Liazoghli, A. Roth, P. Thostrup, D. Colman, Substrate micropatterning as a new in vitro cell culture system to study myelination, ACS Chem. Neurosci. 3 (2012) 90–95.

[8] X. Zhou, A. Yang, Z. Huang, G. Yin, X. Pu, J. Jin, Enhancement of neurite adhesion, alignment and elongation on conductive polypyrrole-poly(lactide acid) fibers with cell-derived extracellular matrix, Colloids Surf., B 149 (2017) 217–225.

[9] G. Hussey, J. Dziki, B.-S. Materials, Extracellular matrix-based materials for regenerative medicine, Nat. Rev. Mat. 3 (2018) 159–173.

[10] I. Song, A. Dityatev, Crosstalk between glia, extracellular matrix and neurons, Brain Res. Bull. 136 (2018) 101–108.

[11] H. Cui, C. Freeman, G. Jacobson, D. Small, Proteoglycans in the central nervous system: role in development, neural repair, and Alzheimer's disease, IUBMB Life 65 (2013) 108–120.

[12] M. Huang, K. Godula, Priming the cellular glycocalyx for neural development, ACS Chem. Neurosci. 5 (2014) 873–875.

[13] M. Singh, B.K. Bachhawat, Isolation and characterization of glycosaminoglycans in human brain of different age groups, J. Neurochem. 15 (1968) 249–258.

[14] R. Richter, N. Baranova, A. Day, J. Kwok, Glycosaminoglycans in extracellular matrix organisation: are concepts from soft matter physics key to understanding the formation of perineuronal nets? Curr. Opin. Struct. Biol. 50 (2018) 65–74.

[15] E. Sterner, L. Meli, S.-J. Kwon, J. Dordick, R. Linhardt, FGF–FGFR signaling mediated through glycosaminoglycans in microtiter plate and cell-based microarray platforms, Biochemistry 52 (2013) 9009–9019.

[16] S. Foscarin, R. Raha-Chowdhury, J.W. Fawcett, J.C.F. Kwok, Brain ageing changes proteoglycan sulfation, rendering perineuronal nets more inhibitory, Aging 9 (2017) 1607–1622.

[17] L. Veillon, C. Fakih, H. Abou-El-Hassan, F. Kobeissy, Y. Mechref, Glycosylation changes in brain cancer, ACS Chem. Neurosci. 9 (2017) 51–72.

[18] L. Bergamaschini, E. Rossi, C. Vergani, M. Simoni, Alzheimer's disease: another target for heparin therapy, Sci. World J. 9 (2009) 891–908.

[19] B. Yang, Y. Chang, A. Weyers, E. Sterner, R. Linhardt, Disaccharide analysis of glycosaminoglycan mixtures by ultra-high-performance liquid chromatography–mass spectrometry, J. Chromatogr. A 1225 (2012) 91–98.

[20] G. Li, L. Li, F. Tian, L. Zhang, C. Xue, R. Linhardt, Glycosaminoglycanomics of cultured cells using a rapid and sensitive LC-MS/MS approach, ACS Chem. Biol. 10 (2015) 1303–1310.

[21] P. Mikael, C. Willard, A. Koyee, C.-G. Barlao, X. Liu, X. Han, et al., Remodeling of glycosaminoglycans during differentiation of adult human bone mesenchymal stromal cells toward hepatocytes, Stem Cell. Dev. 28 (2019) 278–289.

[22] J.C. Silva, X. Han, T. Silva, K. Xia, P. Mikael, J.M.S. Cabral, et al., Glycosaminoglycan remodeling during chondrogenic differentiation of human bone marrow–/synovial-derived mesenchymal stem/stromal cells under normoxia and hypoxia, Glycoconjug J. 37 (2020) 345–360.

[23] Y. Peng, Y. Yu, L. Lin, X. Liu, X. Zhang, P. Wang, et al., Glycosaminoglycans from bovine eye vitreous humour and interaction with collagen type II, Glycoconjug J. 35 (2018) 119–128.

[24] S. Kim, J. Kundu, A. Williams, A. Yandulskaya, J. Monaghan, R. Carrier, et al., Glycosaminoglycans compositional analysis of urodele axolotl (Ambystoma mexicanum) and porcine retina, Glycoconjug J. 36 (2019) 165–174.

[25] J.C. Silva, M.S. Carvalho, X. Han, K. Xia, P.E. Mikael, J.M.S. Cabral, et al., Compositional and structural analysis of glycosaminoglycans in cell-derived extracellular matrices, Glycoconjug J. 36 (2019) 141–154.

[26] Y. Yu, F. Zhang, W. Colón, R. Linhardt, K. Xia, Glycosaminoglycans in human cerebrospinal fluid determined by LC-MS/MS MRM, Anal. Biochem. 567 (2018) 82–84.

[27] J. Hippensteel, R. Uchimido, P. Tyler, R. Burke, X. Han, F. Zhang, et al., Intravenous fluid resuscitation is associated with septic endothelial glycocalyx degradation, Crit. Care 23 (2019) 259.

[28] L. Liang, G. Liu, G. Yu, F. Zhang, R. Linhardt, Q. Li, Urinary metabolomics analysis reveals the anti-diabetic effect of stachyose in high-fat diet/streptozotocin-induced type 2 diabetic rats, Carbohydr. Polym. 229 (2019), 115534.

[29] S. Kim, C. Koetzner, A. Payne, G. Nierode, Y. Yu, R. Wang, et al., Glycosaminoglycan compositional analysis of relevant tissues in zika virus pathogenesis and in vitro evaluation of heparin as an antiviral against zika virus infection, Biochemistry 58 (2019) 1155–1166.

[30] P. Sensharma, G. Madhumathi, R.D. Jayant, A.K. Jaiswal, Biomaterials and cells for neural tissue engineering: current choices, Mater. Sci. Eng. C 77 (2017) 1302–1315.

[31] K. Yang, S. Yu, J. Lee, H.-R. Lee, G.-E. Chang, J. Seo, et al., Electroconductive nanoscale topography for enhanced neuronal differentiation and electrophysiological maturation of human neural stem cells, Nanoscale 9 (2017) 18737–18752.

[32] A. Swaminathan, M. Kumar, S. Sinha, A. Schneider-Anthony, A.-L. Boutillier, T.K. Kundu, Modulation of neurogenesis by targeting epigenetic enzymes using small molecules: an overview, ACS Chem. Neurosci. 5 (2014) 1164–1177.

[33] M.S. Carvalho, J.C. Silva, R.N. Udangawa, J.M.S. Cabral, F.C. Ferreira, C.L. da Silva, et al., Co-culture cell-derived extracellular matrix loaded electrospun microfibrous scaffolds for bone tissue engineering, Mater. Sci. Eng. C 99 (2019) 479–490.

[34] J. Xue, D. Pisignano, Y. Xia, Maneuvering the migration and differentiation of stem cells with electrospun nanofibers, Adv. Sci. (2020), 2000735.

[35] J.C. Silva, M.S. Carvalho, R.N. Udangawa, C.S. Moura, J.M.S. Cabral, C.L. da Silva, et al., Extracellular matrix decorated polycaprolactone scaffolds for improved mesenchymal stem/stromal cell osteogenesis towards a patient-tailored bone tissue engineering approach, J. Biomed. Mater. Res. B Appl. Biomater. 108 (2020).

[36] F.F.F. Garrudo, C.A. Chapman, P.R. Hoffman, R.W. Udangawa, J.C. Silva, P.E. Mikael, et al., Polyaniline-polycaprolactone blended nanofibers for neural cell culture, Eur. Polym. J. 117 (2019) 28–37.

[37] F.F.F. Garrudo, R.N. Udangawa, P.R. Hoffman, L. Sordini, C.A. Chapman, P.E. Mikael, et al., Polybenzimidazole nanofibers for neural stem cell culture, Mater. Today Chem. 14 (2019), 100185.

[38] E. Shahbazi, S. Kiani, H. Gourabi, H. Baharvand, Electrospun nanofibrillar surfaces promote neuronal differentiation and function from human embryonic stem cells, Tissue Eng. 17 (2011) 3021–3031.

[39] J. Corey, C. Gertz, B.-S. Wang, L. Birrell, S. Johnson, D. Martin, et al., The design of electrospun PLLA nanofiber scaffolds compatible with serum-free growth of primary motor and sensory neurons, Acta Biomater. 4 (2008) 863–875.

[40] J. Qu, D. Wang, H. Wang, Y. Dong, F. Zhang, B. Zuo, et al., Electrospun silk fibroin nanofibers in different diameters support neurite outgrowth and promote astrocyte migration, J. Biomed. Mater. Res. 101A (2013) 2667–2678.

[41] F. Garrudo, P.E. Mikael, C. Rodrigues, R.W. Udangawa, P. Paradiso, C.A. Chapman, et al., Polyaniline-polycaprolactone fibers for neural applications: electroconductivity enhanced by pseudo-doping, Mater. Sci. Eng. C (2020), 111680.

[42] M.C.A. de Sousa, C.A.V. Rodrigues, I.A. Ferreira, M.M. Diogo, R.J. Linhardt, J.M.S. Cabral, et al., Functionalization of electrospun nanofibers and fiber alignment enhance neural stem cell proliferation and neuronal differentiation, Front. Bioeng. Biotechnol. 8 (2020), 580135.

[43] D. Nisbet, A. Rodda, M. Horne, J. Forsythe, D. Finkelstein, Neurite infiltration and cellular response to electrospun polycaprolactone scaffolds implanted into the brain, Biomaterials 30 (2009) 4573–4580.

[44] X.F. Kehoe, Boyd Zhang, FDA approved guidance conduits and wraps for peripheral nerve injury: a review of materials and efficacy, Injury 43 (2012) 553–572.

[45] M. Woodruff, D. Hutmacher, The return of a forgotten polymer—polycaprolactone in the 21st century, Prog. Polym. Sci. 35 (2010) 1217–1256.

[46] J.C. Silva, R.N. Udangawa, J. Chen, C.D. Mancinelli, F.F.F. Garrudo, P.E. Mikael, et al., Kartogenin-loaded coaxial PGS/PCL aligned nanofibers for cartilage tissue engineering, Mater. Sci. Eng. C 107 (2019), 110291.

[47] Cipitria, Skelton, Dargaville, Hutmacher Dalton, Design, fabrication and characterization of PCL electrospun scaffolds—a review, J. Mater. Chem. 21 (2011) 9419.

[48] B. Mammadov, M. Sever, M. Guler, A. Tekinay, Neural differentiation on synthetic scaffold materials, Biomater. Sci. UK 1 (2013) 1119–1137.

[49] N. Abbasi, S. Hashemi, M. Salehi, H. Jahani, S. Mowla, M. Soleimani, et al., Influence of oriented nanofibrous PCL scaffolds on quantitative gene expression during neural differentiation of mouse embryonic stem cells, J. Biomed. Mater. Res. 104 (2016) 155–164.

[50] L.M.Y. Yu, N.D. Leipzig, M.S. Shoichet, Promoting neuron adhesion and growth, Mater. Today 11 (2008) 36–43.

[51] F. Pires, Q. Ferreira, C. Rodrigues, J. Morgado, F. Ferreira, Neural stem cell differentiation by electrical stimulation using a cross-linked PEDOT substrate: expanding the use of biocompatible conjugated conductive polymers for neural tissue engineering, Biochim. Biophys. Acta Gen. Subj. 1850 (2015) 1158–1168.

[52] D. Huangfu, K. Osafune, R. Maehr, W. Guo, A. Eijkelenboom, S. Chen, et al., Induction of pluripotent stem cells from primary human fibroblasts with only Oct4 and Sox2, Nat. Biotechnol. 26 (2008) 1269–1275.

[53] K. Takahashi, K. Tanabe, M. Ohnuki, M. Narita, T. Ichisaka, K. Tomoda, et al., Induction of pluripotent stem cells from adult human fibroblasts by defined factors, Cell 131 (2007) 861–872.

[54] S.-Y. Ng, G.K. Bogu, B. Soh, L.W. Stanton, The long noncoding RNA RMST interacts with SOX2 to regulate neurogenesis, Mol. Cell. 51 (2013) 349–359.

[55] V. Graham, J. Khudyakov, P. Ellis, L. Pevny, SOX2 functions to maintain neural progenitor identity, Neuron 39 (2003) 749–765.
[56] R. Donato, E.A. Miljan, S.J. Hines, S. Aouabdi, K. Pollock, S. Patel, et al., Differential development of neuronal physiological responsiveness in two human neural stem cell lines, BMC Neurosci. 8 (2007) 1–11.
[57] Z. Jin, L. Liu, W. Bian, Y. Chen, G. Xu, L. Cheng, et al., Different transcription factors regulate nestin gene expression during P19 cell neural differentiation and central nervous system development, J. Biol. Chem. 284 (2009) 8160–8173.
[58] K.Y. Kwan, J. Shen, D.P. Corey, C-MYC transcriptionally amplifies SOX2 target genes to regulate self-renewal in multipotent otic progenitor cells, Stem Cell Rep. 4 (2015) 47–60.
[59] K. Saied-Santiago, H.E. Bülow, Diverse roles for glycosaminoglycans in neural patterning, Dev. Dynam. 247 (2018) 54–74.
[60] L. Djerbal, H. Lortat-Jacob, J.C. Kwok, Chondroitin sulfates and their binding molecules in the central nervous system, Glycoconjug J. 34 (2017) 363–376.
[61] P. Wassarman, G. Keller, in: Differentiation of Embryonic Stem Cells, first ed., Elsevier Academic Press, 2003.
[62] D. Canning, N. Brelsford, N. Lovett, Chondroitin sulfate effects on neural stem cell differentiation, in Vitro Cell, Dev. Biol. Animal. 52 (2016) 35–44.
[63] C. Flangea, C. Schiopu, E. Sisu, A. Serb, M. Przybylski, D. Seidler, et al., Determination of sulfation pattern in brain glycosaminoglycans by chip-based electrospray ionization ion trap mass spectrometry, Anal. Bioanal. Chem. 395 (2009) 2489.
[64] L. Erskine, C.D. McCaig, Integrated interactions between chondroitin sulphate proteoglycans and weak dc electric fields regulate nerve growth cone guidance in vitro, J. Cell Sci. 110 (1997) 1957–1965.
[65] G. Dick, C. Tan, J. Alves, E. Ehlert, G. Miller, L. Hsieh-Wilson, et al., Semaphorin 3A binds to the perineuronal nets via chondroitin sulfate type E motifs in rodent brains, J. Biol. Chem. 288 (2013) 27384–27395.
[66] R.U. Margolis, R.K. Margolis, L.B. Chang, C. Preti, Glycosaminoglycans of brain during development, Biochemistry 14 (1975) 4797–4804.
[67] A. Suttkus, M. Morawski, T. Arendt, Protective properties of neural extracellular matrix, Mol. Neurobiol. 53 (2016) 73–82.
[68] W. Su, S. Matsumoto, B. Sorg, L. Sherman, Distinct roles for hyaluronan in neural stem cell niches and perineuronal nets, Matrix Biol. 78–79 (2018) 272–283.
[69] S. Back, T. Tuohy, H. Chen, N. Wallingford, A. Craig, J. Struve, et al., Hyaluronan accumulates in demyelinated lesions and inhibits oligodendrocyte progenitor maturation, Nat. Med. 11 (2005) 966–972.
[70] Z.Z. Khaing, S.K. Seidlits, Hyaluronic acid and neural stem cells: implications for biomaterial design, J. Mater. Chem. B 3 (2015) 7850–7866.
[71] P. Milev, P. Maurel, A. Chiba, M. Mevissen, S. Popp, Y. Yamaguchi, et al., Differential regulation of expression of hyaluronan-binding proteoglycans in developing brain: aggrecan, versican, neurocan, and brevican, Biochem. Biophys. Res. Co 247 (1998) 207–212.
[72] M. Herndon, C. Stipp, A. Lander, Interactions of neural glycosaminoglycans and proteoglycans with protein ligands: assessment of selectivity, heterogeneity and the participation of core proteins in binding, Glycobiology 9 (1999) 143–155.
[73] G. Christopherson, H. Song, H.-Q. Mao, The influence of fiber diameter of electrospun substrates on neural stem cell differentiation and proliferation, Biomaterials 30 (2009) 556–564.
[74] J. Tang, C. Wu, S. Chen, Z. Qiao, P. Borovskikh, A. Shchegolkov, et al., Combining electrospinning and electrospraying to prepare a biomimetic neural scaffold with synergistic cues of topography and electrotransduction, ACS Appl. Bio Mater. 3 (2020) 5148–5159.
[75] A. Yang, Z. Huang, G. Yin, X. Pu, Fabrication of aligned, porous and conductive fibers and their effects on cell adhesion and guidance, Colloids Surf. B Biointerfaces 134 (2015) 469–474.
[76] S. Ghafaralahi, M. Ebrahimian-Hosseinabadi, A. Kharazi, Poly(glycerol-sebacate)/poly(caprolactone)/graphene nanocomposites for nerve tissue engineering, J. Bioact. Compat Polym. 33 (2018) 529–542.
[77] V. Mukhatyar, M. Salmerón-Sánchez, S. Rudra, S. Mukhopadaya, T. Barker, A. García, et al., Role of fibronectin in topographical guidance of neurite extension on electrospun fibers, Biomaterials 32 (2011) 3958–3968.
[78] M. Serrano, S. Nardecchia, C. García-Rama, M. Ferrer, J. Collazos-Castro, F. del Monte, et al., Chondroitin sulphate-based 3D scaffolds containing MWCNTs for nervous tissue repair, Biomaterials 35 (2014) 1543–1551.
[79] C.M. Madl, B.L. LeSavage, R.E. Dewi, K.J. Lampe, S.C. Heilshorn, Matrix remodeling enhances the differentiation capacity of neural progenitor cells in 3D hydrogels, Adv. Sci. 6 (2019), 1801716.
[80] F. Li, M. Ducker, B. Sun, F. Szele, J. Czernuszka, Interpenetrating polymer networks of collagen, hyaluronic acid, and chondroitin sulfate as scaffolds for brain tissue engineering, Acta Biomater. 112 (2020) 122–135.